(12)

US ARMY MATERIEL COMMAND

AD

TECHNICAL REPORT BRL-TR-2726

A FAST RESPONSE THERMAL CONDUCTIVITY GAGE

James O. Pilcher, II
Melinda B. Krummerich

April 1986

US ARMY BALLISTIC RESEARCH LABORATORY
ABERDEEN PROVING GROUND, MARYLAND

UNCLASSIFIED

SECURITY CLASSIFICATION OF THIS PAGE (When Data Entered)

REPORT DOCUMENTATION PAGE

READ INSTRUCTIONS BEFORE COMPLETING FORM

1. REPORT NUMBER: Technical Report BRL-TR-2726	2. GOVT ACCESSION NO.: ADA 168185
3. RECIPIENT'S CATALOG NUMBER:	
4. TITLE (and Subtitle): A FAST RESPONSE THERMAL CONDUCTIVITY GAGE	5. TYPE OF REPORT & PERIOD COVERED: FINAL REPORT
6. PERFORMING ORG. REPORT NUMBER:	
7. AUTHOR(s): JAMES O. PILCHER, II MELINDA B. KRUMMERICH	8. CONTRACT OR GRANT NUMBER(s):
9. PERFORMING ORGANIZATION NAME AND ADDRESS: US Army Ballistic Research Laboratory, ATTN: SLCBR-IB Aberdeen Proving Ground, MD 21005-5066	10. PROGRAM ELEMENT, PROJECT, TASK AREA & WORK UNIT NUMBERS:
11. CONTROLLING OFFICE NAME AND ADDRESS: U.S. Army Ballistic Research Laboratory ATTN: SLCBR-DD-T Aberdeen Proving Ground, MD 21005-5066	12. REPORT DATE: April 1986 13. NUMBER OF PAGES: 35
14. MONITORING AGENCY NAME & ADDRESS (if different from Controlling Office):	15. SECURITY CLASS. (of this report): UNCLASSIFIED 15a. DECLASSIFICATION DOWNGRADING SCHEDULE:

16. DISTRIBUTION STATEMENT (of this Report)

Approved for Public Release; Distribution Unlimited.

17. DISTRIBUTION STATEMENT (of the abstract entered in Block 20, if different from Report)

18. SUPPLEMENTARY NOTES

19. KEY WORDS (Continue on reverse side if necessary and identify by block number)

Thermocouple
Thermal fluence gage
Heat flux
Heat deposition

20. ABSTRACT (Continue on reverse side if necessary and identify by block number) jmk

During the spring of 1983, the Ballistic Research Laboratory measured behind-the-armor effects for several weapons against a variety of targets. The generation of heat inside the target during and following impact was a primary concern. Off-the-shelf thermal gages did not meet the requirements of quick response and durability in a severe environment, so the authors developed and manufactured a thermal fluence gage.

(continued on next page)

DD FORM 1 JAN 73 1473 EDITION OF 1 NOV 65 IS OBSOLETE

UNCLASSIFIED

SECURITY CLASSIFICATION OF THIS PAGE (When Data Entered)

20. (continued)

Performance of the gage in the laboratory and in the field is discussed. The design details and possible modifications are also presented.

TABLE OF CONTENTS

LIST OF ILLUSTRATIONS

I. INTRODUCTION

During the spring of 1983, the Ballistic Research Laboratory measured behind-the-armor effects for several weapons against a variety of targets. One of the major concerns was heat generation during and immediately following impact of the warhead against the targets.

Previous tests of this type had used thin skin total heat gages and standard laboratory heat detectors. Thin skin gages record only the maximum temperature attained by skins' back surface with no indication of the time required to reach this temperature. Although an approximation of the total heat deposition can be made, no rate of deposition can be estimated without knowing the time of the event. The large thermal mass of a typical laboratory detector such as an infrared power meter is designed to measure a steady-state flux and cannot respond quickly enough to register a transient event. Neither gage type can withstand severe blast and shock environments.

Since the temperature inside the target rose sharply in a very short time, special gages were fabricated which emphasized the time response of the gage rather than its thermal capacity. This gage is used when the thermal flux is of short duration, 150 milliseconds or less, and of low total energy, 179 Calories per square centimeter or less. The maximum operating temperature of the gage is 500 degrees Celsius.

II. GAGE DESCRIPTION

A. Basic Gage Configuration

The basic configuration of the thermal conductivity gage is shown in Figure 1. The measuring element of the gage is a thin aluminum disc with a

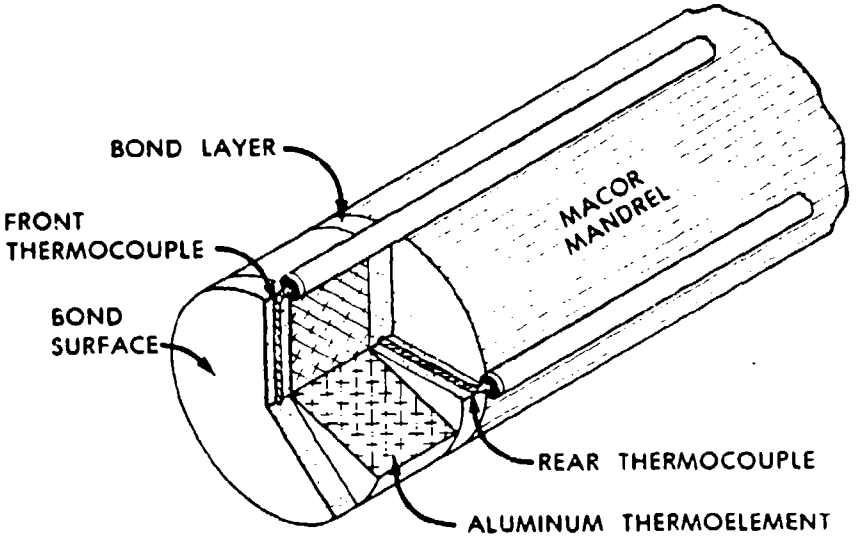

Figure 1. Basic Thermal Conductivity Gage Configuration

chromel-alumel thermocouple mounted across the center of each face using a thermoconducting epoxy. This subassembly is mounted on the end of a ceramic mandrel which is inserted into the ceramic sleeve so that the front surface of the disc is flush with the front of the sleeve. Wires connecting the gage to any external instrumentation are anchored to the mandrel and then passed out the rear of the sleeve. Detailed drawings of the gage are in the Appendix.

B. Design Calculations

Based on the following assumptions and material properties, gage performance was calculated from the general one-dimensional thermal conductivity equation,

$$\partial T/\partial t = a\partial^2 T/\partial x^2 \qquad (1)$$

where

T = temperature in degrees Celsius;
t = time in seconds;
a = thermal diffusivity in square centimeters per second; and
x = distance in centimeters.

The equation was solved by the graphical method described in Reference 1 and illustrated in Figure 2. Time response of the gage was calculated by plotting temperature distribution versus time as heat passes longitudinally through the different materials in the gage in constant differential increments of time. This differential time element and the incremental distance through the gage are related by

$$\Delta x^2 = a\Delta t. \qquad (2)$$

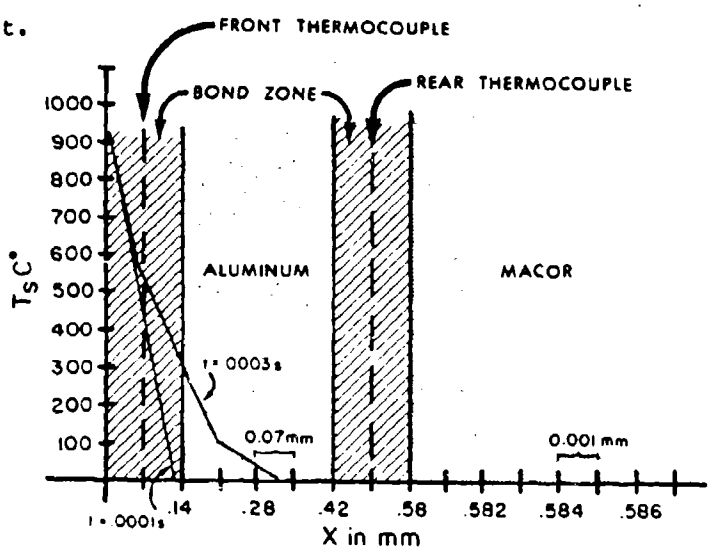

Figure 2. Thermal Geometry for Calculation

1 M. Jakob, G.E. Hawkins, Elements of Heat Transfer, John Wiley & Sons, Inc., New York, 1958.

1. **Assumptions.** The following assumptions were used in the calculations.

a. The heat flow in and out of the gage is parallel to the longitudinal axis of the gage. Heat flow in the radial direction is insignificant.

b. The cement used to bond the thermocouples to the disc has conductive properties similar to aluminum. The thickness of the bond is approximately one wire diameter.

c. The temperature measured by the thermocouples is assumed to be the average temperature in the bond layers.

d. The primary sources of heat are radiant in nature, so film and boundary layer effects are ignored in calculating the thermal response characteristics. These effects retard convective and conductive heat transfer but do not significantly influence radiant heat transfer.

e. The thermocouple wires are of sufficiently small cross section and of sufficient length to render heat loss from the gage insignificant (0.076 millimeters in diameter and 30 millimeters long).

2. **Material Properties.** The disc is manufactured from 2024-T4 aluminum alloy. Both the mounting mandrel and the surrounding sleeve were fabricated from Macor, an alumina-based, machinable ceramic. Density, thermal conductivity, and specific heat were obtained from the cited literature. Thermal diffusivity is determined by the relation

$$a = k/\rho C_p \quad . \tag{3}$$

The 2024-T4 aluminum properties are:[2]

density (ρ) = 0.135 gm/cm^2;
thermal conductivity (k) = 2.64 Cal/cm sec°C;
specific heat (C_p) = 32.8 Cal/gm°C; and
thermal diffusivity (a) = 0.597 cm^2/sec.

The Macor properties are:[3]

ρ = 0.125 gm/cm^2;
k = 3.1 x 10^{-3} Cal/cm sec°C;
C_p = 180 to 200 Cal/gm°C; and
a = 0.11 to 0.12 x 10^{-3} cm^2/sec.

2 D.A. Maykuth, Aerospace Structural Metals Handbook, Belfour Stulen, Inc., Columbus, OH, 1960.

3 Corning Bulletin, "Macor Machinable Glass Ceramic," Corning Glass Works, Corning, NY, 1981.

The disc is 0.0305 centimeters wide and has a diameter of 0.625 centimeters. The thermocouple wire diameter and the bond layer thickness are both 0.0076 centimeters.

3. Response Calculation Results. The geometry in Figure 2 and the above stated material properties were used in the graphical solution of Eq. (1) for the conditions of changing surface temperature and conduction layers of differing materials. Figure 3 shows the response of the front thermocouple to a surface temperature step rise of one millisecond and Figure 4 shows the response of the same thermocouple to a 250 Hertz sinusoidal surface temperature variation. The shaded portions of the curves show the uncertainty in the calculations due to variations of the actual material properties and vagaries introduced by the assumptions.

4. Calculation of Flux Density. The flux density (q') is the sum of the instantaneous conductive heat flow density (q'_f) and the differential heat storage density (q'_s) . These quantities are defined by the following equations:

$$q' = q'_f + q'_s \ \text{Cal/cm}^2\text{sec}; \tag{4}$$

$$q'_f = k\Delta T/\Delta x \ \text{Cal/cm}^2\text{sec}; \tag{5}$$

$$q'_s = (\rho C_p/2)(\Delta T_1/\Delta t + \Delta T_2/\Delta t)\Delta x \ \text{Cal/cm}^2\text{sec}; \tag{6}$$

where T_1 is the front thermocouple temperature and T_2 is the rear thermocouple temperature. The linearity shown in the above equations is true for steady-state heat flow and for sufficiently small values of Δx. By combining Eqs. (4), (5), and (6), the following equation is derived for total flux density:

$$q' = (k/\Delta x)(T_1 - T_2) + (\rho C_p \Delta x/2)(\Delta T_1/\Delta t + \Delta T_2/\Delta t) \ \text{Cal/cm}^2\text{sec}; \tag{7}$$

where Δx (= 0.044 cm) is the distance between the two thermocouples. Evaluating the constants in Eq. (7) yields

$$q' = 50.0(T_1 - T_2) + 0.097(\Delta T_1/\Delta t + \Delta T_2/\Delta t) \ \text{Cal/cm}^2\text{sec}. \tag{8}$$

5. Calculation of Total Deposition Density. The total heat deposition (Q') is the time integral of the flux density (q').

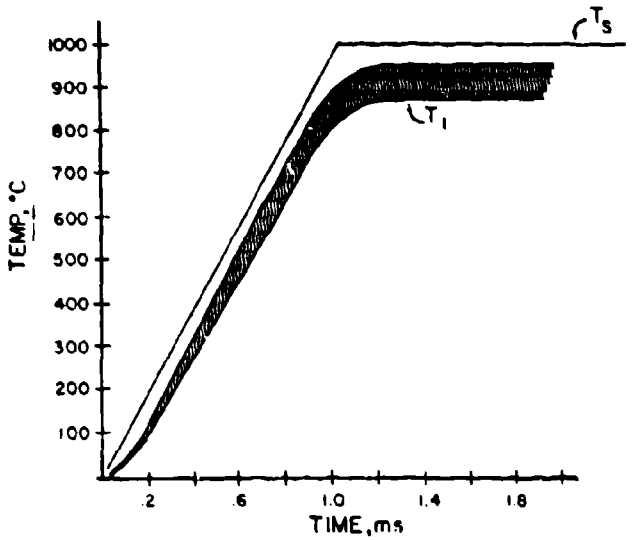

Figure 3. Response of Front Thermocouple to Step Function

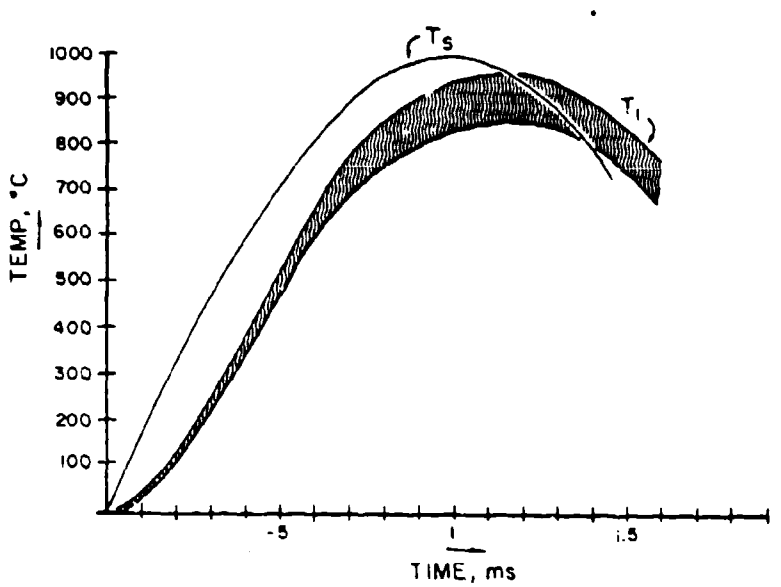

Figure 4. Response of Front Thermocouple to 250 Hertz Sinusoidal Function

$$Q' = \int_{t_o}^{t_f} q'dt \ \text{Cal/cm}^2; \tag{9}$$

where $(t_f - t_o)$ is the time interval of observation. This integration yields

$$Q' = 60.0\int_{t_o}^{t_f}(T_1 - T_2)dt + 0.097(T_1 + T_2)\Big|_{t_o}^{t_f} \ \text{Cal/cm}^2. \tag{10}$$

The interval of interest for both thermocouples is the time between the first rise from the baseline temperature (t_o) and the point at which the maximum temperature is reached (t_f) by the front thermocouple. Since the integration zero time is taken at the start of the event, reference junctions in the data acquisition system are unnecessary as long as the changes in temperature are referenced with respect to the temperature at time t_o.

6. **Approximate Solutions.** Since the measurand is a transient and the aft portion of the gage has a much lower thermal conductivity than the front portion of the gage, the deposition and flux density are actually nonlinear and of the forms:

$$q' = F\{(T_1 - T_2), (\Delta T_1/\Delta t + \Delta T_2/\Delta t)\} \ \text{Cal/cm}^2\text{sec}, \tag{11}$$

and

$$Q' = G\{\int_{t_o}^{t_f}(T_1 - T_2)dt, (T_1 + T_2)\} \ \text{Cal/cm}^2 . \tag{12}$$

The existence of significant levels of interference in the data acquired from the field make Eqs. (11) and (12) quite cumbersome to evaluate. Simpler algorithms can be developed based on the limits of Eqs. (11) and (12) in the time domain and least squares fits to calibration data.

From Eq. (11), it becomes evident that for short time intervals, the average temperature in the gage becomes the dominant parameter. The flux density can be expressed as:

$$q' = F\{(\Delta T_1/\Delta t + \Delta T_2/\Delta t)/2\} \text{ Cal/cm}^2\text{sec}, \quad (13)$$

and the total deposition as:

$$Q' = G\{(\Delta T_1 + \Delta T_2)/2\} \text{ Cal/cm}^2, \quad (14)$$

where

$\Delta T_1 = T_{1_f} - T_{1_o}$ over the time interval Δt;

$\Delta T_2 = T_{2_f} - T_{2_o}$ over the time interval Δt; and

$\Delta t = t_f - t_o$, the time interval.

These approximations resemble the equations for thin skin gages, except for the introduction here of a time variable.

III. GAGE CALIBRATION

A. Calibration Procedure

The gage was calibrated by comparing its output to the radiant energy output of a carbon dioxide laser operating at 10.6 micrometers. A fast-response photon drag detector was used to measure the laser energy directly; the laser energy was also calculated from the laser output power and the time duration of the pulse. The power is constant for any one calibration trial and the pulse time is equivalent to the current input time. The gage outputs were recorded through data amplifiers into a transient recording oscilloscope. The recording components were calibrated against a digital voltage standard both individually and as a system. Figure 5 shows the apparatus used in the calibration.

B. Apparatus

The following is the list of equipment used in the calibration procedure.

1. CO_2 Laser: Apollo Lasers Inc., Model 500, serial number 101.
2. Infrared Power Meter: Coherent Radiation Laboratories Inc., detector serial number 081.

3. Germanium Focusing Lens: Coherent Radiation Laboratories, Inc., 10 inch focal length, no serial number.

4. Transient Recording Oscilloscope: Nicolet Corp., Model Explorer II, serial number 612831.

5. Instrumentation Amplifiers: Dynamics Inc. Model 7525, serial numbers 3543 and 3563.

6. DC Voltage Standard: Analogic Inc., Model AN3100, serial number 7825476.

7. Photon Drag Detector: Rotin, Inc., Model 741D, serial number 081.

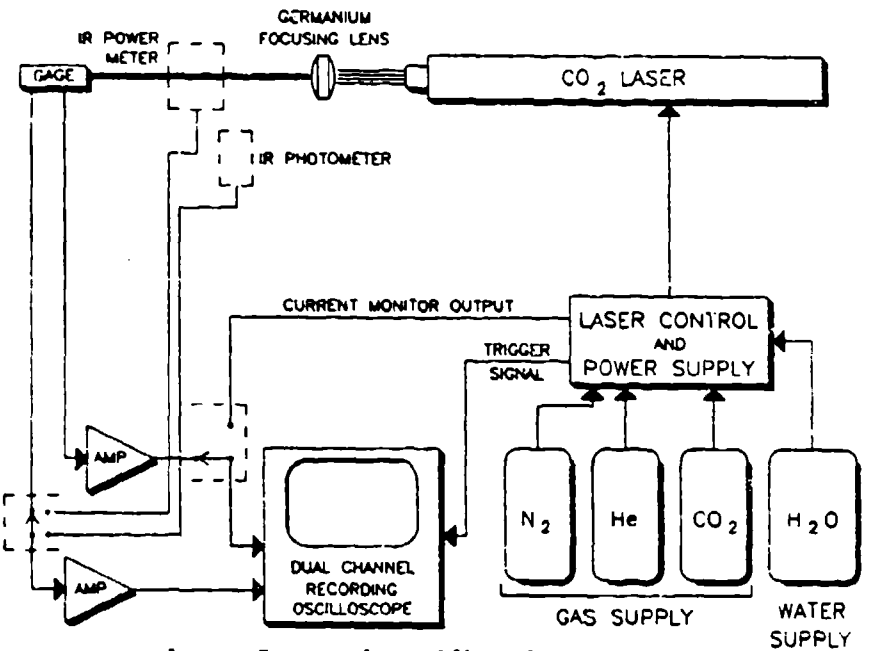

Figure 5. Basic Calibration Set Up

C. Recording System Calibration

The recording system was calibrated on site, in three separate steps.

First, the recording oscilloscope was calibrated against the voltage standard on both channels A and B over all ranges. These calibrations, performed in accordance with the manufacturer's instructions, included both the recording and the playback systems. This procedure must be completed before calibrating the instrumentation amplifiers.

Next, the instrumentation amplifiers were calibrated for zero, balance, linearity, and gain using the manufacturer's procedures as outlined in the equipment manual. The voltage standard was used as the reference.

Finally, the acquisition and recording system was assembled as it was to be used during the tests and checked for ground loop and noise interference. A ten-step voltage pulse was recorded on every track of each channel. The pulses were stored on floppy disc and later used to establish calibration and conversion coefficients for data analysis.

Figure 6 shows the recording system calibration scheme.

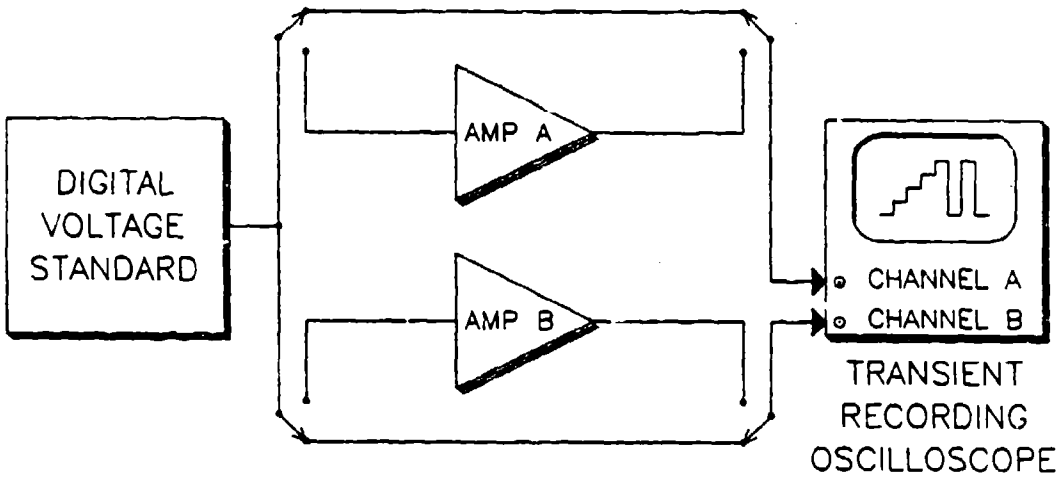

Figure 6. Recording System Calibration Scheme

The overall system accuracy was:

Linearity - 0.2% full scale;
Amplitude Resolution - 0.05% full scale;
Time Resolution - 0.2% range;
Amplifier Gain - 100 + 0.02%.

D. Laser Calibration

Since the laser output cannot be monitored without disturbing the beam, the laser was calibrated by determining the relationship between output radiation and input current. The photon drag detector provided the output data and the laser control panel's current monitor supplied both the input data and the triggering pulse to the recording system. In both the single pulse and the multipulse modes, the duration of the output pulse was about 250 microseconds less than that of the current pulse. The output pulse showed a delay of about 50 microseconds from the input pulse.

For each calibration test series, the laser beam was focused over the active area of the temperature gage. The gage was then removed and the beam

placed in multipulse mode. The energy delivered by each pulse was calculated using the average power, the frequency, and the period of the duty cycle. The power was measured by the infrared meter and the last two quantities determined by the photon drag detector.

Figure 7 shows a schematic of the calibration setup.

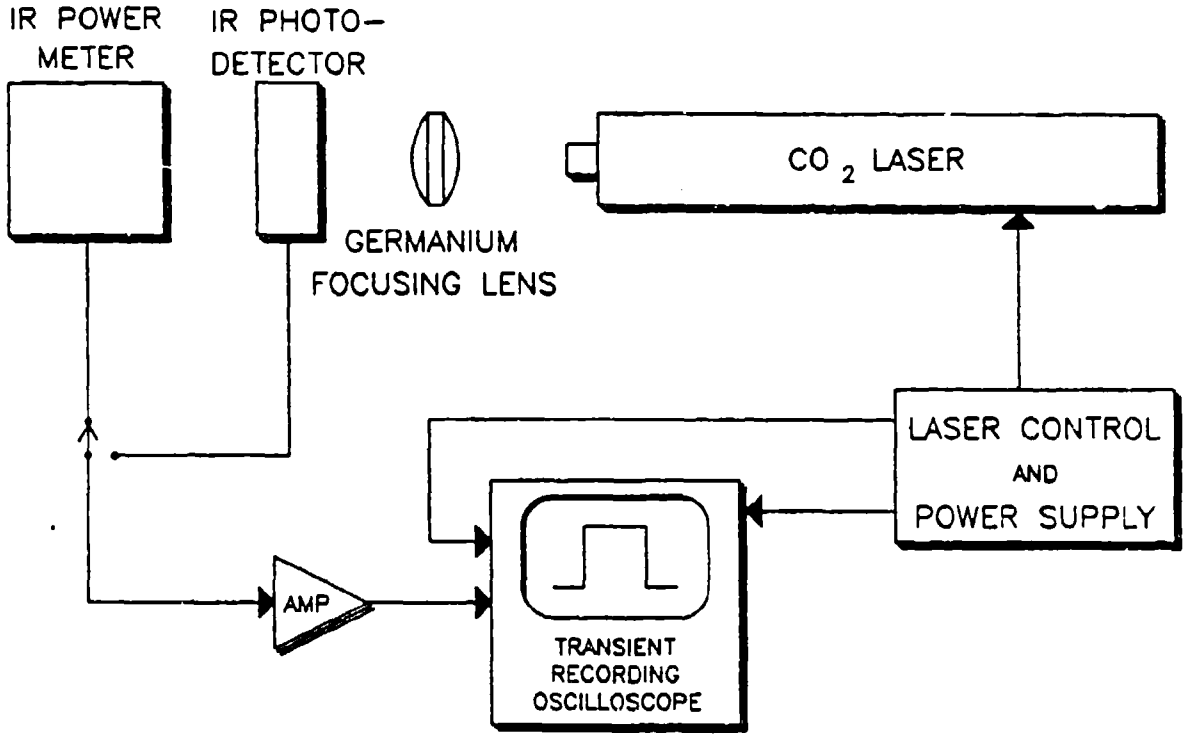

Figure 7. Laser System Calibration Scheme

E. Gage Calibration

Once the laser output parameters were established, the test gage was inserted into the beam as shown in Figure 8. The gage output voltages were recorded for both single and multipulse modes. Figures 9 and 10 show the typical gage response to a single pulse and to multiple pulses, respectively.

The results of the calibration trials are shown in Figure 11.

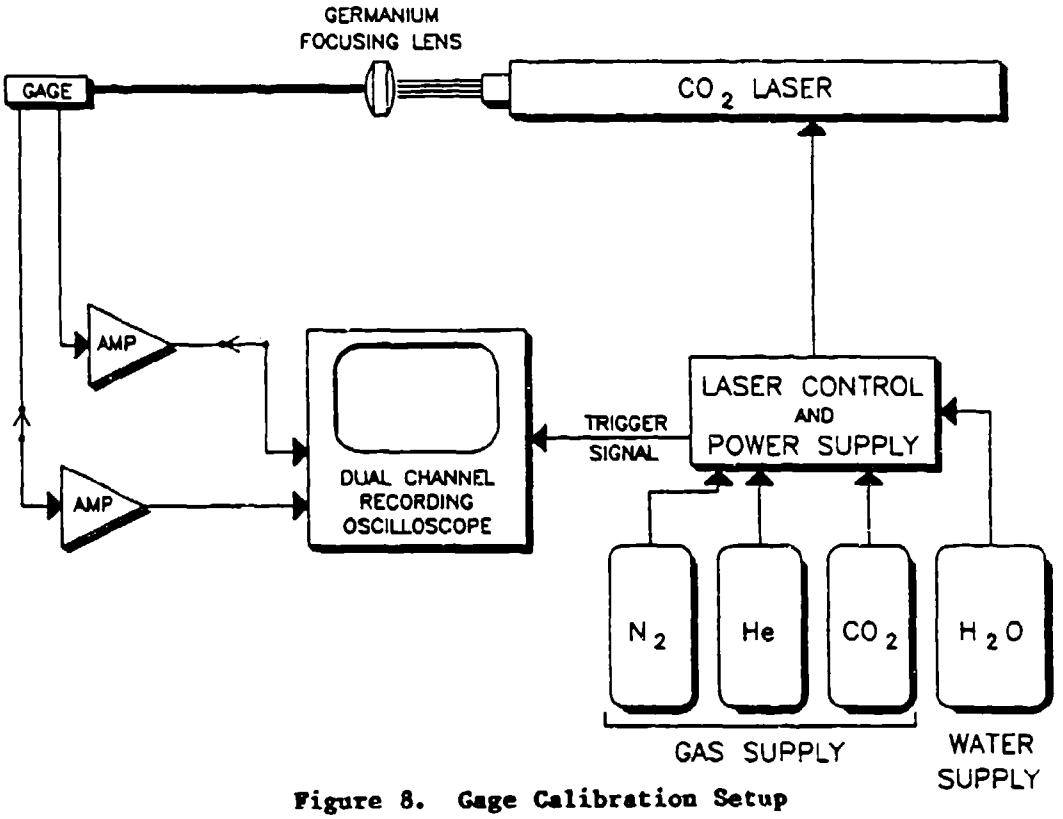

Figure 8. Gage Calibration Setup

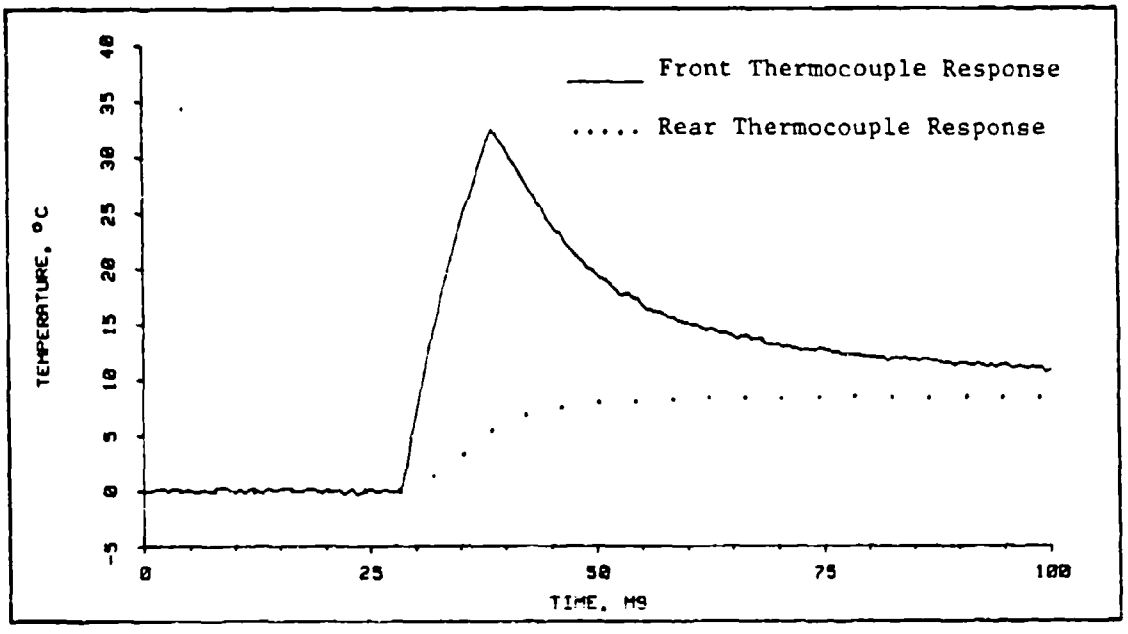

Figure 9. Typical Gage Response to Single Laser Pulse

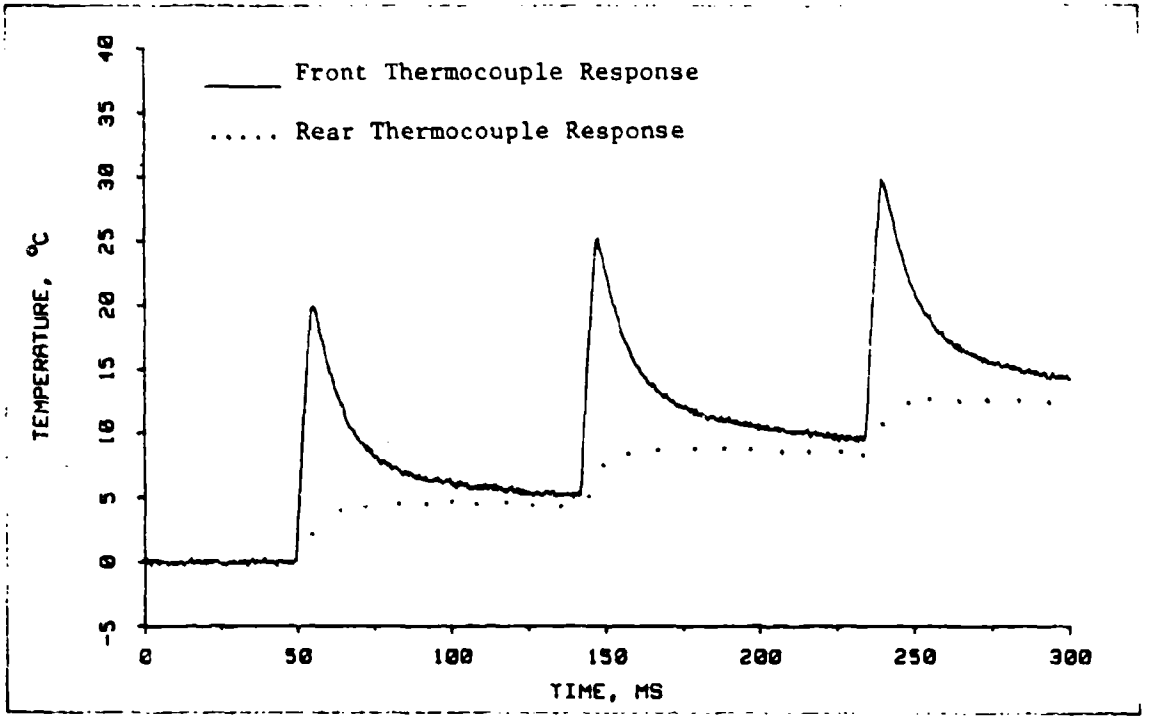

Figure 10. Typical Gage Response to Multiple Laser Pulses

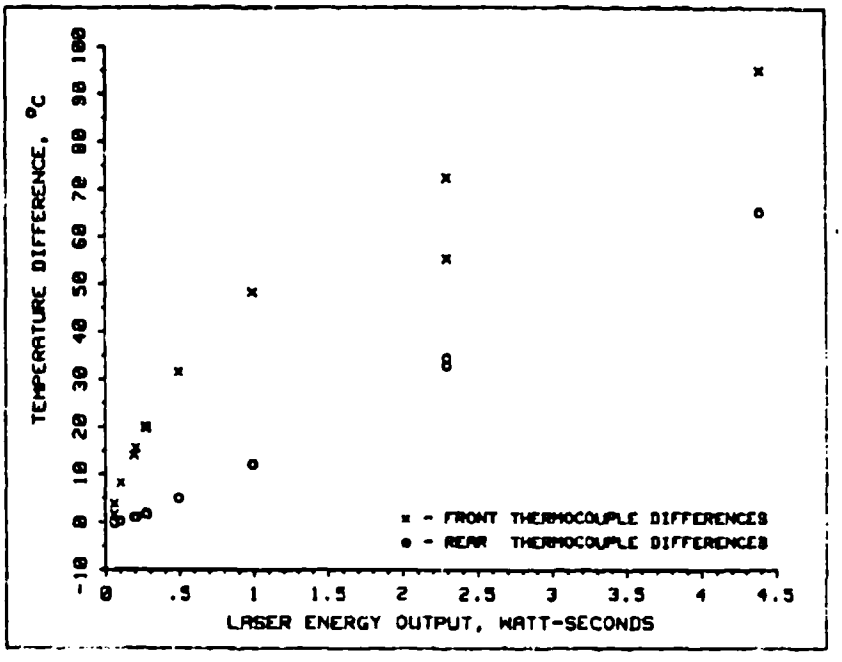

Figure 11. Data Points For Calibration

IV. RESULTS

A. Gage Response

The operating response of the gage ranged from one to 250 milliseconds. Pulses shorter than one millisecond could not be measured, and pulses longer than 250 milliseconds caused saturation of the gage, with full saturation occurring at about 200 milliseconds.

Figures 12 and 13 show typical field measurements for the front and rear thermocouples. The calculation shown in Figures 3 and 4 indicates that the actual peak surface temperature of the gage can be 20% higher than the front thermocouple measures. This discrepancy is larger during the pulse's rise. Because of this uncertainty in the measured temperatures, the approximations for heat flux density and heat deposition yielded only average values over the interval Δt shown in Figures 12 and 13.

B. Evaluation of Heat Flux Density

The approximation for flux density, Eq. (13), and the analytical relation, Eq. (7), do not describe the gage operation well. This is due to the extreme sensitivity of differentiation to signal noise and to discontinuities caused by digitization. A satisfactory estimate of the average flux density was obtained by dividing the total deposition by the time of deposition, Δt:

$$q' = Q'/\Delta t \ \text{Cal/cm}^2\text{sec} \qquad (15)$$

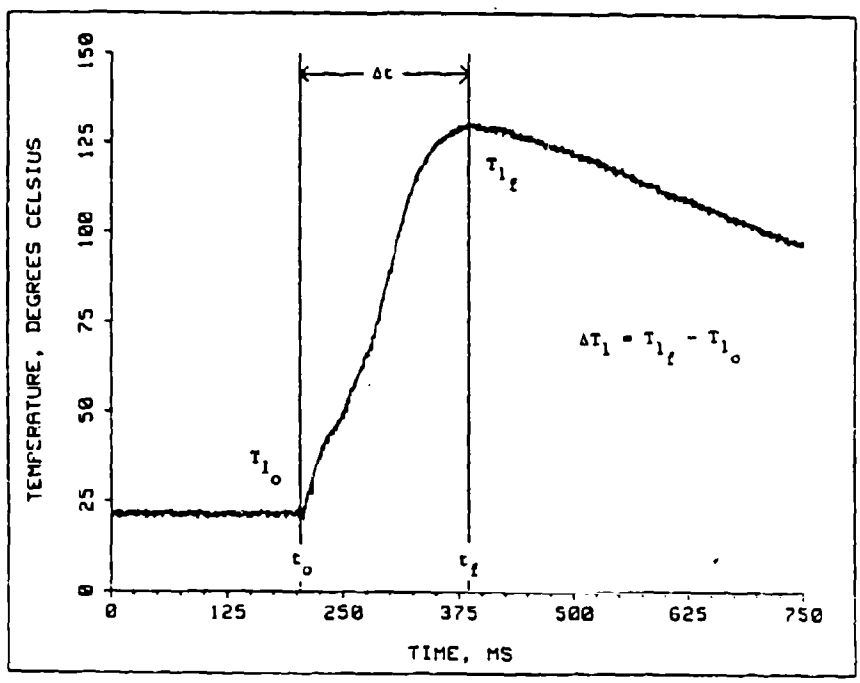

Figure 12. Typical Field Measurement by Front Thermocouple

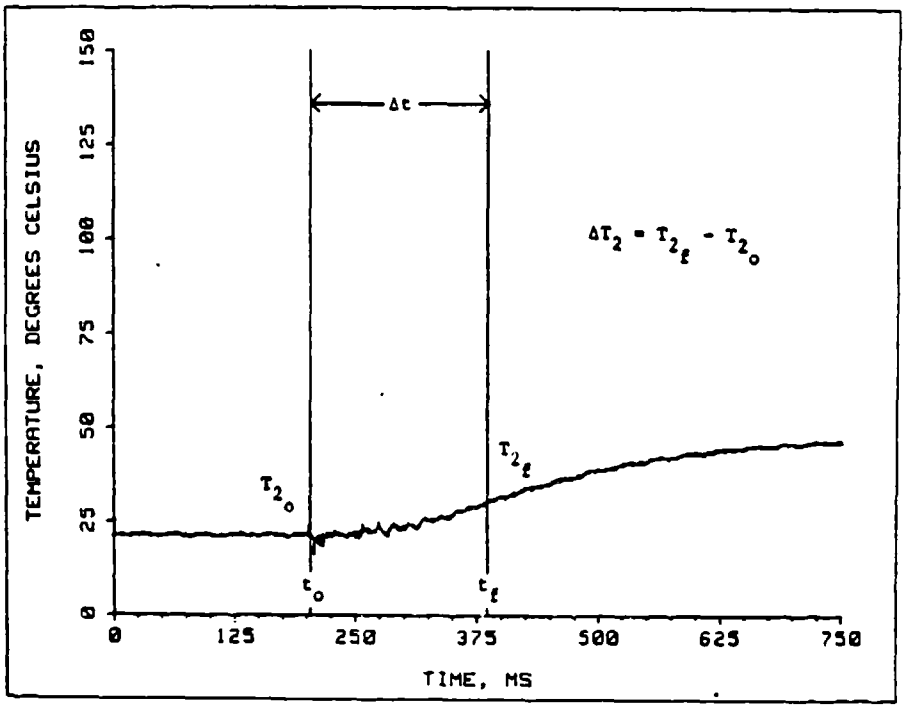

Figure 13. Typical Field Measurement by Rear Thermocouple

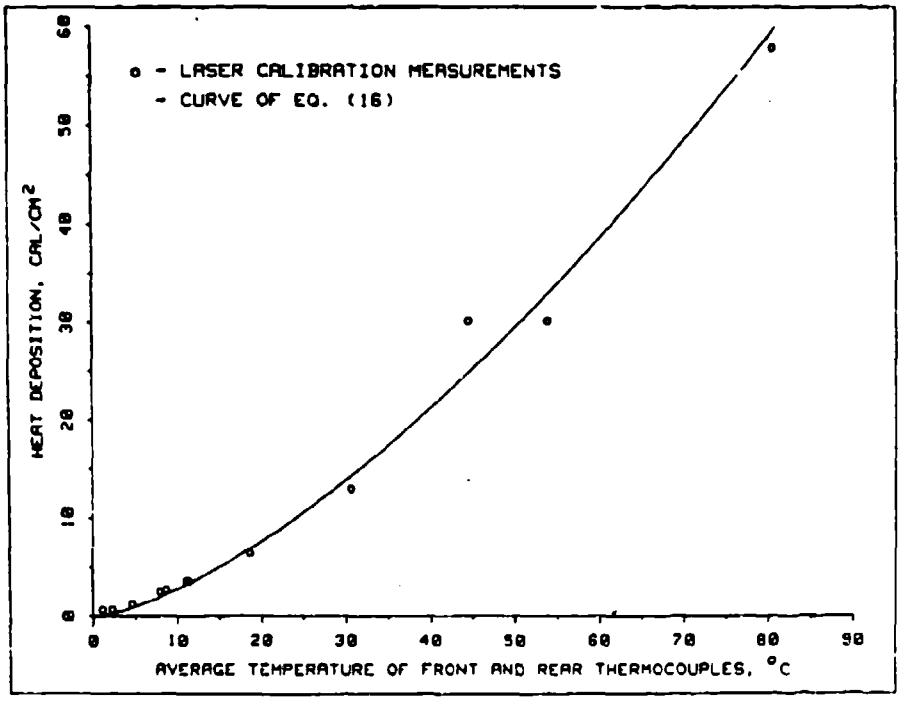

Figure 14. Comparison of the Calculated Heat Deposition with the Measured Values

C. Evaluation of Heat Deposition

The approximation for heat deposition, Eq. (14), provided a reasonable description of the gage operation. Least squares calculations showed the deposition density function and its coefficients to be

$$Q' = 0.0918 \left[\frac{\Delta T_1 + \Delta T_2}{2}\right]^{1.4759} \quad \text{Cal/cm}^2, \tag{16}$$

where ΔT_1 and ΔT_2 were determined as shown in Figures 12 and 13. Figure 14 compares this calculated deposition density with the measured data.

V. CONCLUSIONS

The gage as presently constituted performs reasonably well as a thermal flux gage, although design changes could simplify both the data acquisition and analysis. Such changes include adoption of a two-wire shielded thermocouple and vapor-deposited thermocouple junctions. The two-wire system would reduce the number of necessary data channels to one per gage, thus eliminating the differencing step in the analysis. Use of the vapor-deposited junctions would allow more accurate measurement of the gage surface temperature.

REFERENCES

1. M. Jakob, G. E. Hawkins, Elements of Heat Transfer, John Wiley & Sons, Inc., New York, 1958.

2. D. A. Maykuth, Aerospace Structural Metals Handbook, Belfour Stulen, Inc., Columbus, Ohio, 1980.

3. Corning Bulletin, "Macor Machinable Glass Ceramic," Corning Glass Works, Corning, N.Y., 1981.

APPENDIX

Figures A1 through A5 are detailed engineering drawings of the gage fully assembled and its constituent parts.

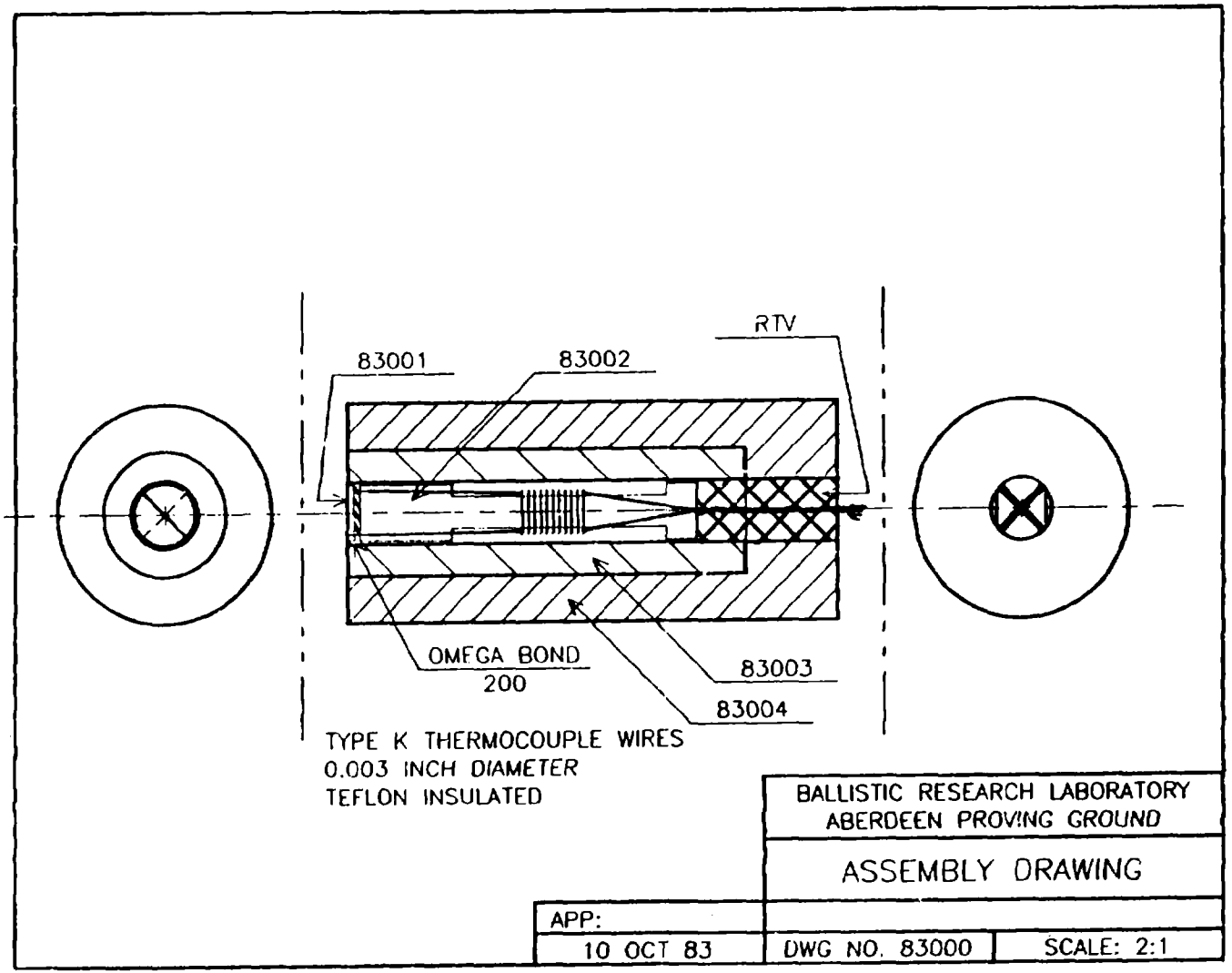

Figure A-1. Assembly of Thermal Conductivity Cage

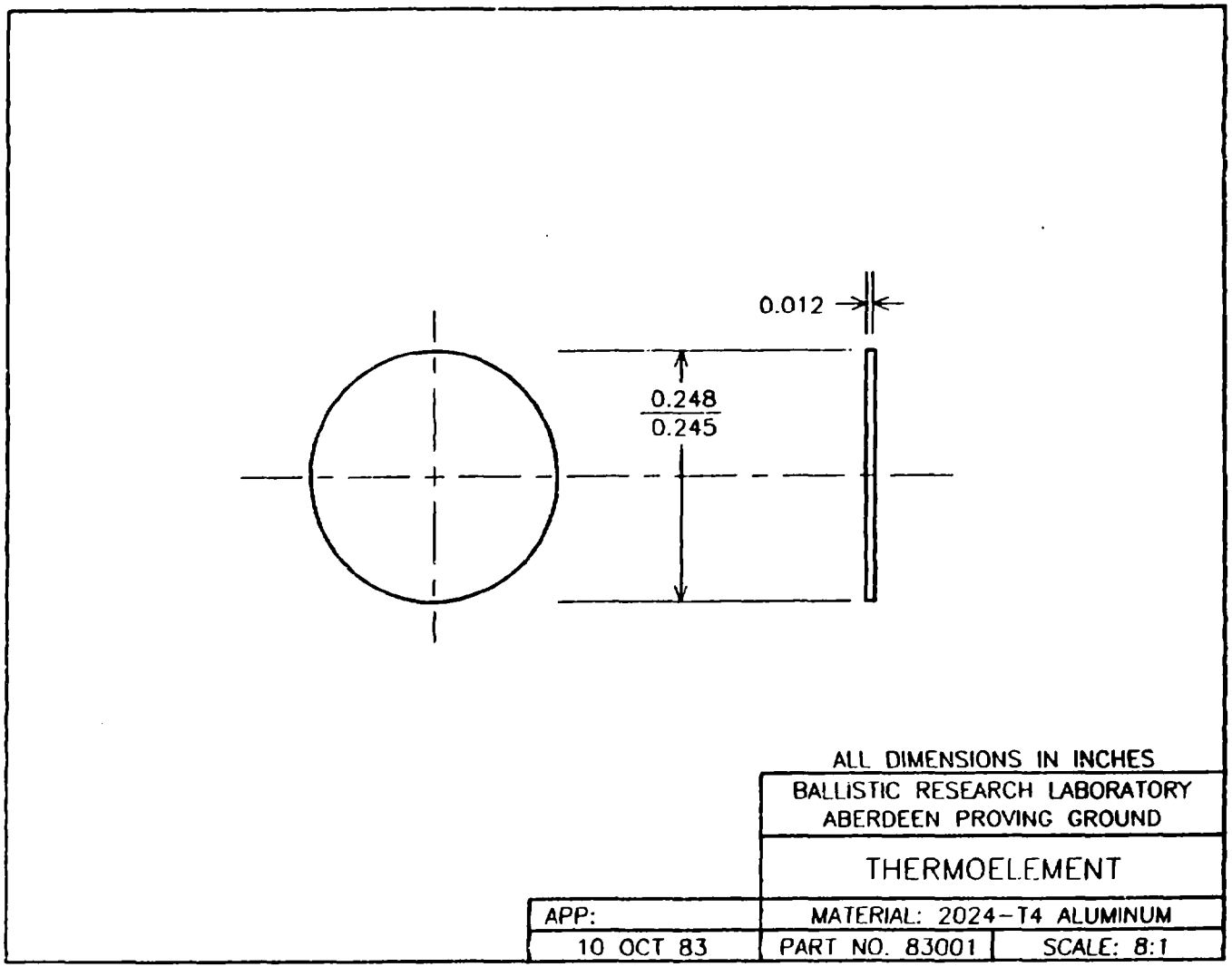

Figure A-2. Gage Thermoelement

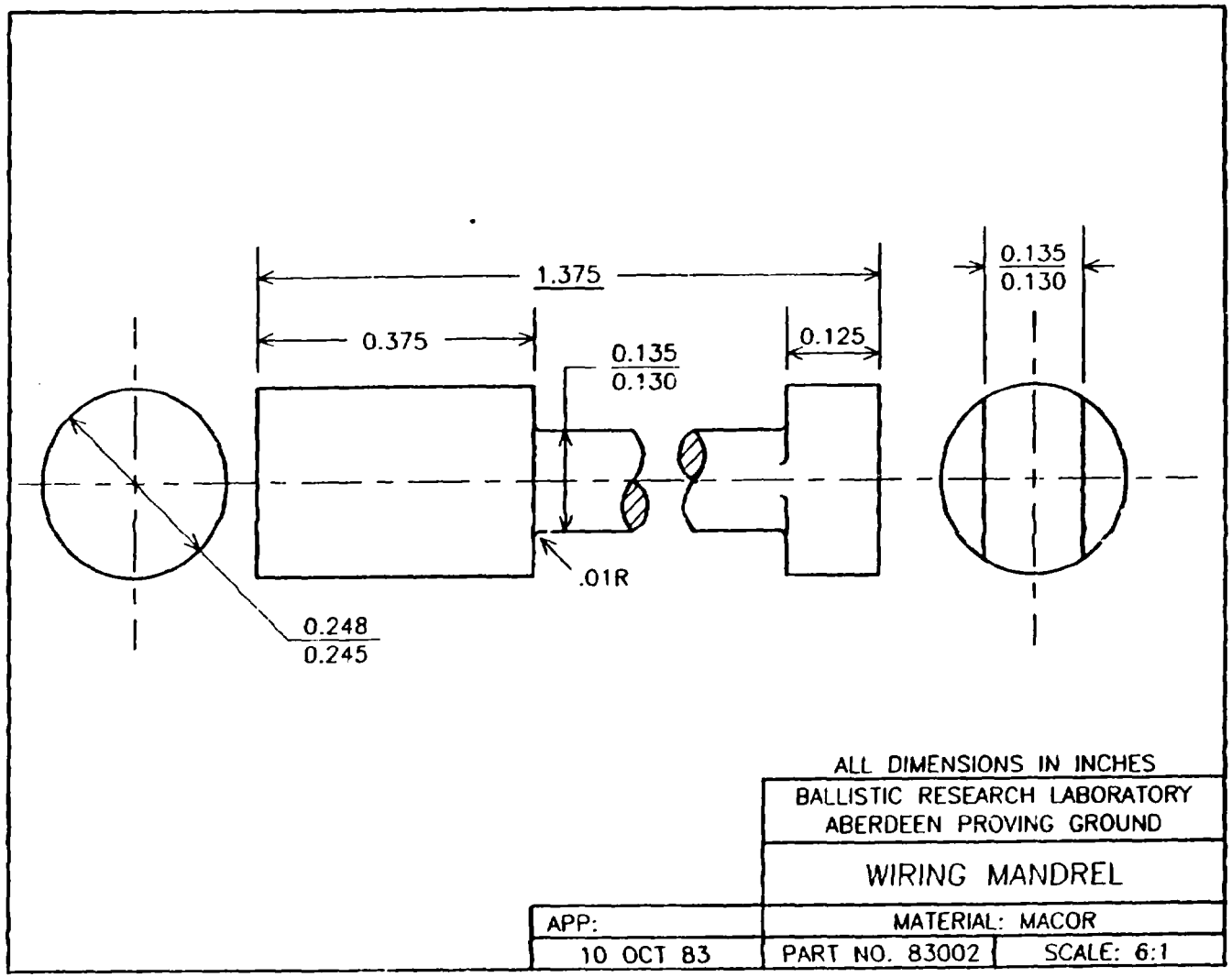

Figure A-3. Thermocouple Wiring Mandrel

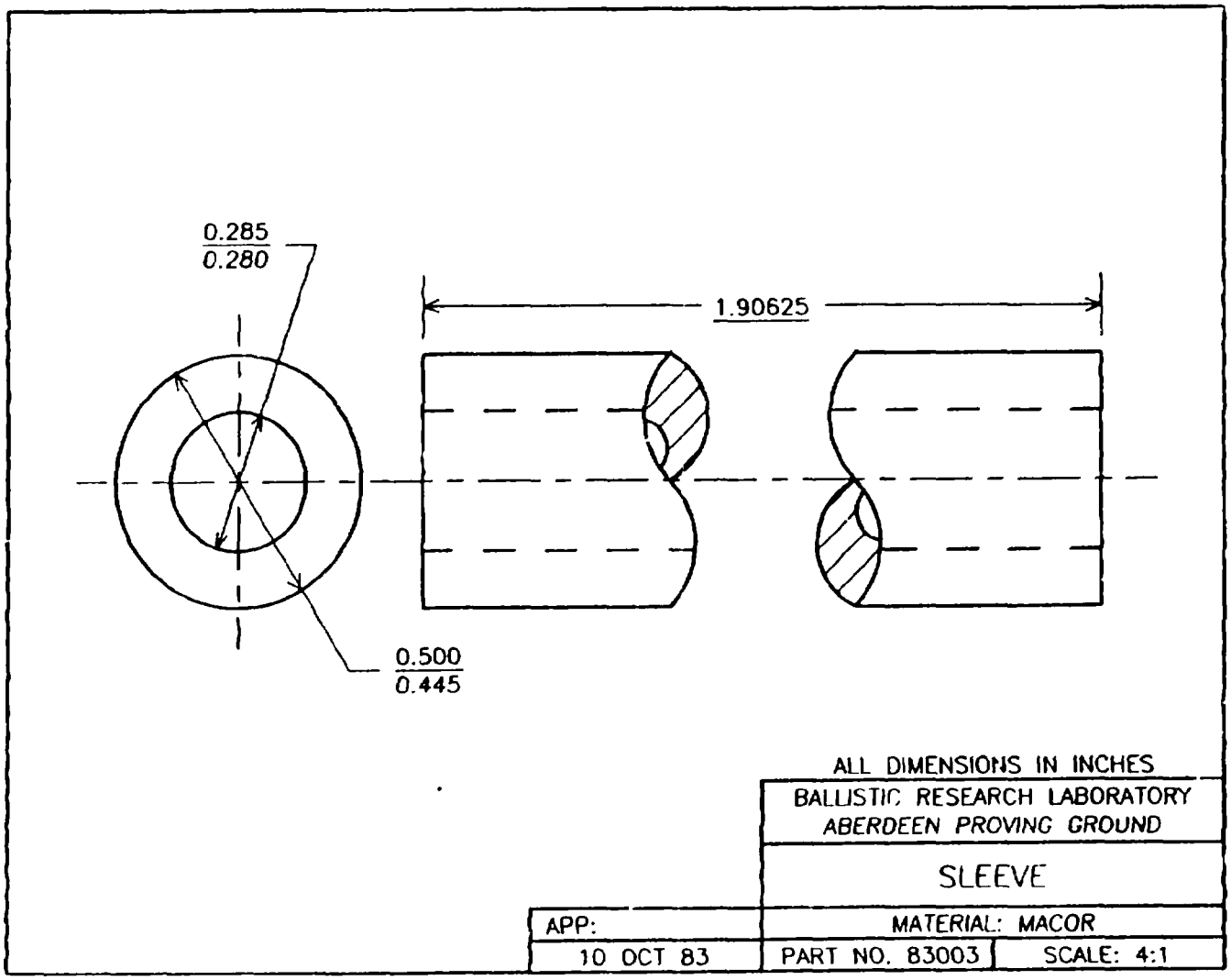

Figure A-4. Mandrel Sleeve

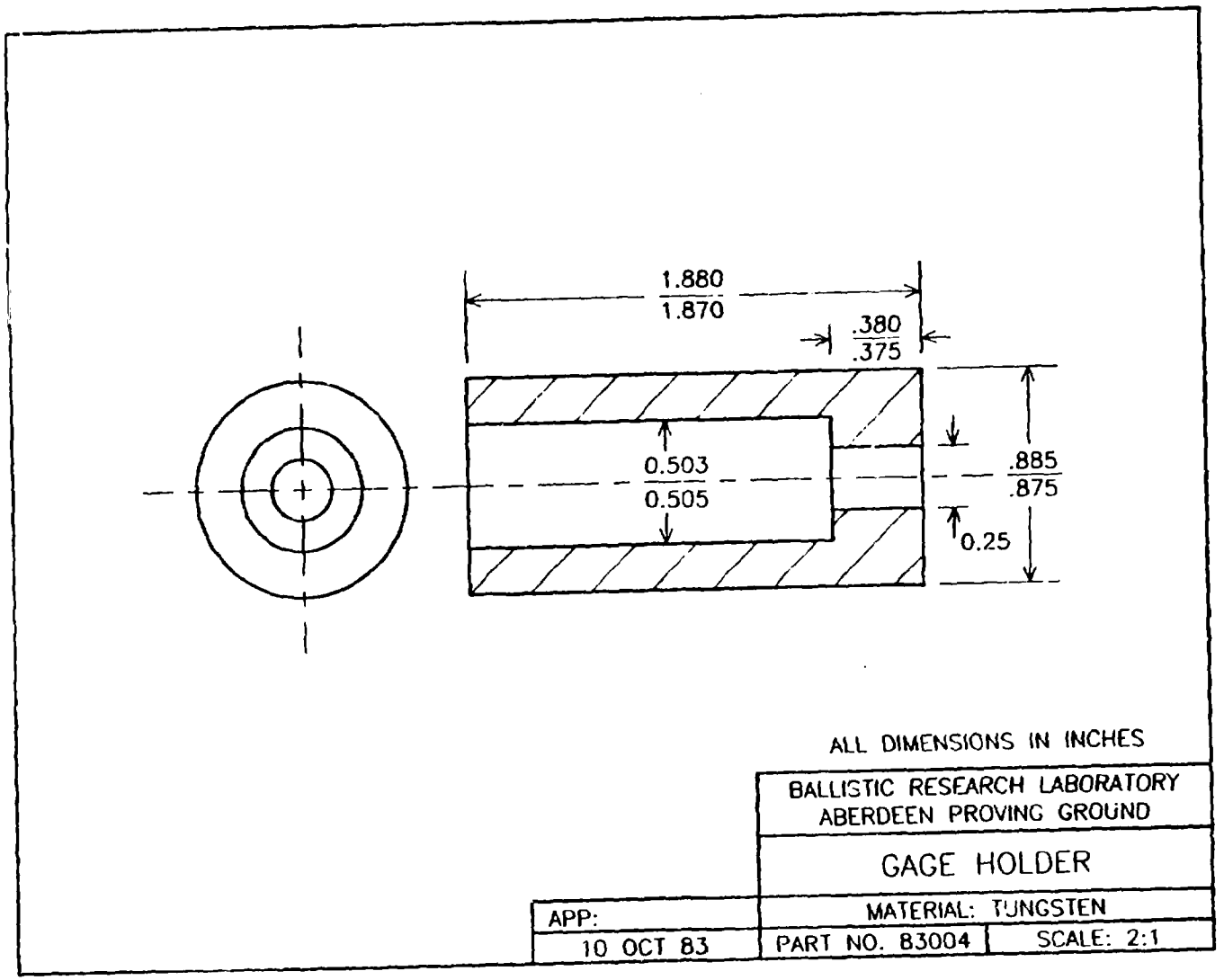

Figure A-5. Gage Holder

DISTRIBUTION LIST

No. of Copies	Organization
12	Administrator Defense Technical Info Center ATTN: DTIC-DDA Cameron Station Alexandria, VA 22304-6145
1	HQDA DAMA-ART-M Washington, D.C. 20310
1	Commander U.S. Army Materiel Command ATTN: AMCDRA-ST 5001 Eisenhower Avenue Alexandria, VA 22333-0001
1	Commander Armament R&D Center US Army AMCCOM ATTN: SMCAR-TSS Dover, NJ 07801
1	Commander Armament R&D Center US Army AMCCOM ATTN: SMCAR-TDC Dover, NJ 07801
1	Director Benet Weapons Laboratory Armament R&D Center US Army AMCCOM ATTN: SMCAR-LCB-TL Watervliet, NY 12189
1	Commander US Army BMD Advanced Technology Center ATTN: BMDATC-M, Mr. P. Boyd P.O. Box 1500 Huntsville, AL 35804
1	Commander U.S. Army Materiel Command ATTN: AMCLDC, J. Bender 5001 Eisenhower Avenue Alexandria, VA 22333-0001

No. of Copies	Organization
3	Commander US Army AMCCOM, ARDC Dover, NJ 07801
5	Commander US Army AMCCOM, ARDC ATTN: SMCAR-SCM SMCAR-SCS, B. Brodman SMCAR-SCS, T. Hung SMCAR-SCA, W. Gadomski SMCAR-SCA, E. Malatesta Dover, NJ 07801
1	Commander US Army AMCCOM, ARDC ATTN: Product Assuranc Directorate SMCAR-QAR-RIB, D. IMHOF Dover, NJ 07801
1	Commander US Army Armament, Munitions and Chemical Command ATTN: SMCAR-ESP-L Rock Island, IL 61299
1	Commander US Army Aviation Research and Development Command ATTN: AMSAV-E 4300 Goodfellow Blvd. St. Louis, MO 63120
1	Director US Army Air Mobility Research and Development Laboratory Ames Research Center Moffett Field, CA 94035
1	Commander US Army Communications Electronics Command ATTN: AMSEL-ED Fort Monmouth, NJ 07703
1	Commander ERADCOM Technical Library ATTN: DELSD-L (Rpcs Section) Fort Monmouth, NJ 07703-5301

DISTRIBUTION LIST

No. of Copies	Organization
1	Commander US Army Missile Command Research, Development and Engineering Center ATTN: AMSMI-RD Redstone Arsenal, AL 35898-5500
1	Director US Army Missile and Space Intelligence Center ATTN: AIAMS-YDL Redstone Arsenal, AL 35898-5500
1	Director US Army TRADOC Systems Analysis Activity ATTN: ATAA-SL WSMR, NM 88002
1	Commandant US Army Infantry School ATTN: ATSH-CD-CSO-OR Fort Benning, GA 31905
1	Commander US Army Development and Employment Agency ATTN: MODE-TED-SAB Fort Lewis, WA 98433
1	AFWL/SUL Kirtland, AFB, NM 87117
1	Air Force Armament Laboratory ATTN: AFATL/DLODL Eglin AFB, FL 32542-5000
1	Commander US Army Tank Automotive Cmd ATTN: AMSTA-TSL Warren, MI 48397-5000
1	Product Manager for 30mm Ammo. ATTN: AMCPM-AAH-30mm Dover, NJ 07801
2	Director US Army Materials and Mechanics Research Center ATTN: J. Mescall Tech. Library Watertown, MA 02172
2	Commander Naval Sea Systems Command (SEA-62R41) ATTN: L. Pasiuk Washington, DC 20362
1	Commander Naval Explosive Ordnance Disposal Facility ATTN: Lib Div Indian Head, MD 20640
1	Superintendent Naval Postgraduate School ATTN: Dir of Lib Monterey, CA 93940
1	Commander Naval Weapons Center ATTN: Code 3431, Tech Lib China Lake, CA 93555
4	AFATL Gun and Rocket Division Gun Test Branch AD3246 TEST W/TETFG ATTN: W. Dittrich; DLJM D. Davis; DLDL Eglin AFB, FL 32542
1	AFELM, The Rand Corporation ATTN: Library-D 1700 Main Street Santa Monica, CA 90406
1	Hughes Helicopter Inc. ATTN: Richard E. Knapp Centinela & Teale Streets Mail Station T-2113 Culver City, CA 90230

DISTRIBUTION LIST

No. of Copies	Organization
10	Central Intelligence Agency Office of Central Reference Dissemination Branch Room GE-47 HQS Washington, D.C. 20502

Aberdeen Proving Ground, MD

Dir, USAMSAA
ATTN: AMXSY-D
AMXSY-MP, H. Cohen

Cdr, USATECOM
ATTN: AMSTE-TO-F

Cdr, CRDCE, AMCCOM
ATTN: SMCCR-RSP-A
SMCCR-MU
SMCCR-SPS-IL

Dir, DRSTE-SG-H, Mr. Cole
Mr. Witt

USER EVALUATION SHEET/CHANGE OF ADDRESS

This Laboratory undertakes a continuing effort to improve the quality of the reports it publishes. Your comments/answers to the items/questions below will aid us in our efforts.

1. BRL Report Number_____ Date of Report_____

2. Date Report Received_____

3. Does this report satisfy a need? (Comment on purpose, related project, or other area of interest for which the report will be used.)_____

4. How specifically, is the report being used? (Information source, design data, procedure, source of ideas, etc.)_____

5. Has the information in this report led to any quantitative savings as far as man-hours or dollars saved, operating costs avoided or efficiencies achieved, etc? If so, please elaborate._____

6. General Comments. What do you think should be changed to improve future reports? (Indicate changes to organization, technical content, format, etc.)

CURRENT ADDRESS

Name

Organization

Address

City, State, Zip

7. If indicating a Change of Address or Address Correction, please provide the New or Correct Address in Block 6 above and the Old or Incorrect address below.

OLD ADDRESS

Name

Organization

Address

City, State, Zip

(Remove this sheet along the perforation, fold as indicated, staple or tape closed, and mail.)